
This is an electronic reprint of the original article.
This reprint may differ from the original in pagination and typographic detail.

Halli, Petteri; Wilson, Benjamin P.; Hailemariam, Taye; Latostenmaa, Petri; Yliniemi, Kirsi; Lundström, Mari

Electrochemical recovery of tellurium from metallurgical industrial waste

Published in:
Journal of Applied Electrochemistry

DOI:
[10.1007/s10800-019-01363-6](https://doi.org/10.1007/s10800-019-01363-6)

Published: 01/01/2020

Document Version
Publisher's PDF, also known as Version of record

Published under the following license:
CC BY

Please cite the original version:
Halli, P., Wilson, B. P., Hailemariam, T., Latostenmaa, P., Yliniemi, K., & Lundström, M. (2020). Electrochemical recovery of tellurium from metallurgical industrial waste. *Journal of Applied Electrochemistry*, 50(1), 1-14. <https://doi.org/10.1007/s10800-019-01363-6>



Electrochemical recovery of tellurium from metallurgical industrial waste

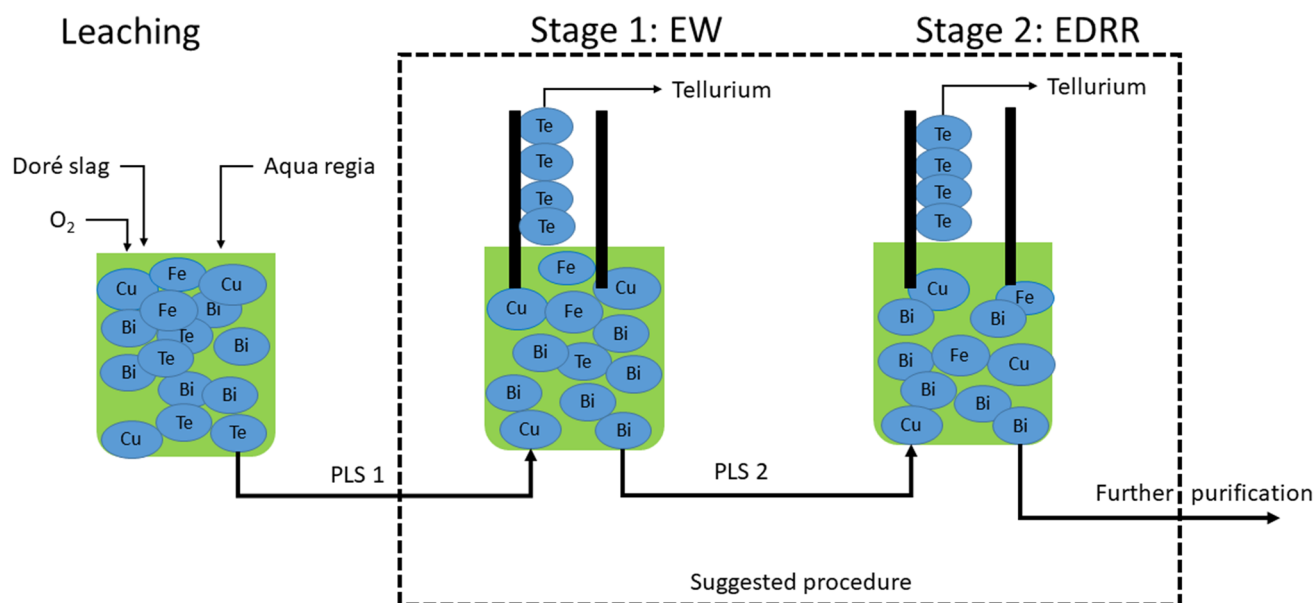
Petteri Halli¹ · Benjamin P. Wilson¹ · Taye Hailemariam¹ · Petri Latostenmaa² · Kirsi Yliniemi³ · Mari Lundström¹

Received: 24 May 2019 / Accepted: 24 October 2019 / Published online: 8 November 2019
© The Author(s) 2019

Abstract

The current study outlines the electrochemical recovery of tellurium from a metallurgical plant waste fraction, namely Doré slag. In the precious metals plant, tellurium is enriched to the TROF (Tilting, Rotating Oxy Fuel) furnace slag and is therefore considered to be a lost resource—although the slag itself still contains a recoverable amount of tellurium. To recover Te, the slag is first leached in aqua regia, to produce multimetal pregnant leach solution (PLS) with 421 ppm of Te and dominating dissolved elements Na, Ba, Bi, Cu, As, B, Fe and Pb (in the range of 1.4–6.4 g dm⁻³), as well as trace elements at the ppb to ppm scale. The exposure of slag to chloride-rich solution enables the formation of cuprous chloride complex and consequently, a decrease in the reduction potential of elemental copper. This allows improved selectivity in electrochemical recovery of Te. The results suggest that electrowinning (EW) is a preferred Te recovery method at concentrations above 300 ppm, whereas at lower concentrations EDRR is favoured. The purity of recovered tellurium is investigated with SEM–EDS (scanning electron microscope–energy dispersion spectroscopy). Based on the study, a new, combined two-stage electrochemical recovery process of tellurium from Doré slag PLS is proposed: EW followed by EDRR.

Graphic abstract



Keywords EDRR · EW · Circular economy of metals · Doré slag

✉ Mari Lundström
mari.lundstrom@aalto.fi

Extended author information available on the last page of the article

1 Introduction

Tellurium is a metalloid element [1], which is currently produced primarily as a by-product of copper electrorefining via anode slime treatment [2, 3]. It is commonly used in solar panels [4–6], production of thermoelectric materials [6–8], semiconductors [9, 10] and as an alloying element in metals like steel to improve the machinability [6, 11]. Although tellurium is mainly produced as a side product of a base metal industry [2, 3], the growth of large-scale renewable energy generation, particularly use of solar panels, has resulted in an increased demand for Te [12, 13]. The conventional way to recover tellurium metal is to treat the anode slime via a number of combined hydro- and pyrometallurgical stages, e.g. pressure leaching in an acidic and/or alkaline environment [3, 14–17]. Nevertheless, as the Doré process—normally carried out in a TROF (Tilting, Rotating Oxy Fuel) furnace—uses treated anode slime as a raw material, any tellurium remaining in the slime distributes to the slag and is considered to be an irretrievable resource [18, 19]. Due to the increased pressure on the world's natural resources, it is essential that the loss of even minor amounts of critical and valuable elements is avoided in order to promote more sustainable behaviour. Therefore, the ability to recover even minor concentrations of economically significant or critical elements, like tellurium, is essential according to the principles of the materials circular economy.

The slag produced in the Doré process typically includes B, Fe, Ba, Pb, Na and Si, which originates from the added slag formers, whereas Bi, Cu, Se, Te, PM (precious metals) and PGM (platinum group metals) that result from anode slimes are also often found at minor concentrations. Consequently, any methodology that leads to improved recovery from copper anode slimes could have a significant impact on the overall environmental and economic sustainability of a base metal smelter process. The current study addresses this challenge by focusing on the recovery of Te via the application of electrodeposition-redox replacement (EDRR) and electrowinning (EW). These methods—when combined—offer the opportunity to decrease Te wastage whilst enhancing the overall sustainability of tellurium production.

During the ED step of the EDRR process, only a very thin (porous) layer of a sacrificial metal is deposited and this formed metal layer is then spontaneously replaced by a more noble metal during the redox replacement (RR) step, without the use of any externally applied potential or current, i.e. energy. The impetus for the redox replacement reactions between two or more reactive metals is driven by the difference between their standard potentials [20–30]. This is not only the basic principle of EDRR

(electrodeposition-redox replacement) but also of similar methods like surface-limited redox replacement (SLRR) [29–32] and electrochemical atomic layer deposition (e-ALD) [33–36]; the main difference is that in SLRR and e-ALD thin, defect free monolayers are formed via underpotential deposition, whereas in EDRR more porous films grow on the surface. In contrast, electrowinning (EW) relies on the direct electroplating of the desired metal element on the electrode surface—by the application of the appropriate potential or current—to produce a surface layer. To date, the EDRR method has been employed for metal reclamation, including Ag recovery from synthetic Zn process solutions [37–39], Au recovery from synthetic cyanide-free cupric chloride leaching solutions [39, 40] and Pt recovery from synthetic and real industrial nickel solutions [41, 42]. Nevertheless, there are no previous reports related to the recovery of Te by EDRR, or even more, combining the electrowinning (EW) and EDRR sequentially to maximise the recovery. This paper demonstrates how both EDRR and EW are employed as part of a comprehensive investigation into the recovery of Te from a Doré slag pregnant leach solution (PLS).

2 Experimental procedure

2.1 Raw material

The Doré slag leachates, i.e. PLS employed in this work, were obtained by treating industrial Doré slag with 30% aqua regia following a previously described procedure [43]. The composition of the investigated Te-containing multi-metal PLS was obtained by both ICP-OES (inductively coupled plasma–optical emission spectroscopy, Thermo Fisher Scientific iCAP 6500 Duo, USA) and ICP-MS (inductively coupled plasma–mass spectroscopy, Thermo Fisher Scientific iCAP Qc, USA) as shown in Table 1. The analyses were performed in triplicate and the average concentrations are reported. The 65% HNO₃ and 37% HCl (both VWR Chemicals, Belgium) used were of technical grade, whereas the metal content for the synthetic solutions was provided by the appropriate AAS standards (Te, As, Ag, Bi, Cu, Pb and Fe, 1000 mg dm^{−3}, Sigma-Aldrich, USA). All solutions were made to the desired concentration using deionised water (Merck Millipore, USA). The electrode surfaces after the EDRR or EW experiments were analysed by scanning electron microscope, (SEM, Mira³ Tescan GM, Czech Republic) with coupled energy dispersion spectroscopy (EDS, Thermo Scientific UltraDry, USA) using an acceleration voltage of 15 keV. A total of 6 to 8 point spectra were taken along with two to four 25 µm × 25 µm area analyses and averages of the spectra obtained are presented as wt% values.

Table 1 Composition of investigated Doré slag PLS as determined by ICP-OES (g/L and ppm) and ICP-MS (ppb)

As (g dm ⁻³)	B (g dm ⁻³)	Ba (g dm ⁻³)	Bi (g dm ⁻³)	Cu (g dm ⁻³)	Fe (g dm ⁻³)	Na (g dm ⁻³)	Pb (g dm ⁻³)
3.7	3.1	5.1	4.6	3.9	1.4	6.4	1.4
Al (ppm)	Ca (ppm)	K (ppm)	Mg (ppm)	Ni (ppm)	Sb (ppm)	Sn (ppm)	Te (ppm)
508	256	77	920	177	365	345	421
Ag (ppm)	Co (ppm)	Cr (ppm)	In (ppm)	Mn (ppm)	Se (ppm)	Ti (ppm)	Zn (ppm)
54	9.3	16	6.3	11	1.2	1.8	52
	Cd (ppb)	Pt (ppb)	Ga (ppb)	Ge (ppb)	Au (ppb)	Pd (ppb)	
	390	30	120	40	115	188	

Table 2 EDRR parameters investigated, E_1 =deposition potential, E_2 =cut-off potential, t_1 =deposition time, t_2 =cut-off time and n =amount of cycles

Parameter	Value
E_1 [mV vs. SCE]	− 500, − 300, − 100, +100
E_2 [mV vs. SCE]	− 50, +50, +150
t_1 [s]	2
t_2 [s]	1000
n	100

Table 3 EW parameters investigated, E =deposition potential and t =deposition time

Parameter	Value
Te in solution [ppm]	400, 300, 200, 100, 50, 25, 20, 15, 10, 1
E [mV vs. SCE]	− 600, − 500, − 360, − 245, +75, +150, +250
t [s]	200

2.2 Cell set-up

Electrochemical measurements were conducted with a standard three-electrode cell set-up comprised of a reference saturated calomel electrode (SCE, B521, SI Analytics, Germany), 0.1-mm-thick ($A = 24 \text{ cm}^2$) Pt plate as a counter electrode (CE) and 0.1-mm-thick ($A = 0.24\text{--}0.4 \text{ cm}^2$) Pt plate as a working electrode (WE, both Kultakeskus, Finland). The cell set-up was controlled using an IviumStat 24-bit CompactStat potentiostat (Ivium Technologies, The Netherlands) and is described in more detail elsewhere [37–41]. **N.B.** All subsequent potentials detailed are versus SCE unless otherwise stated.

2.3 EDRR measurements

The EDRR parameters investigated are outlined in Table 2 and only one parameter was modified at a time during the measurements. The next EDRR cycle started when either cut-off time (t_2) or cut-off potential (E_2) was reached, whichever occurred first.

2.4 EW experiments

The investigated EW parameters are presented in Table 3. Additionally, a set of extended EW experiments of 1200-s

duration were conducted at the same potentials (Table 3) using PLS solution derived from the aqua regia leaching of industrial Doré slags [43].

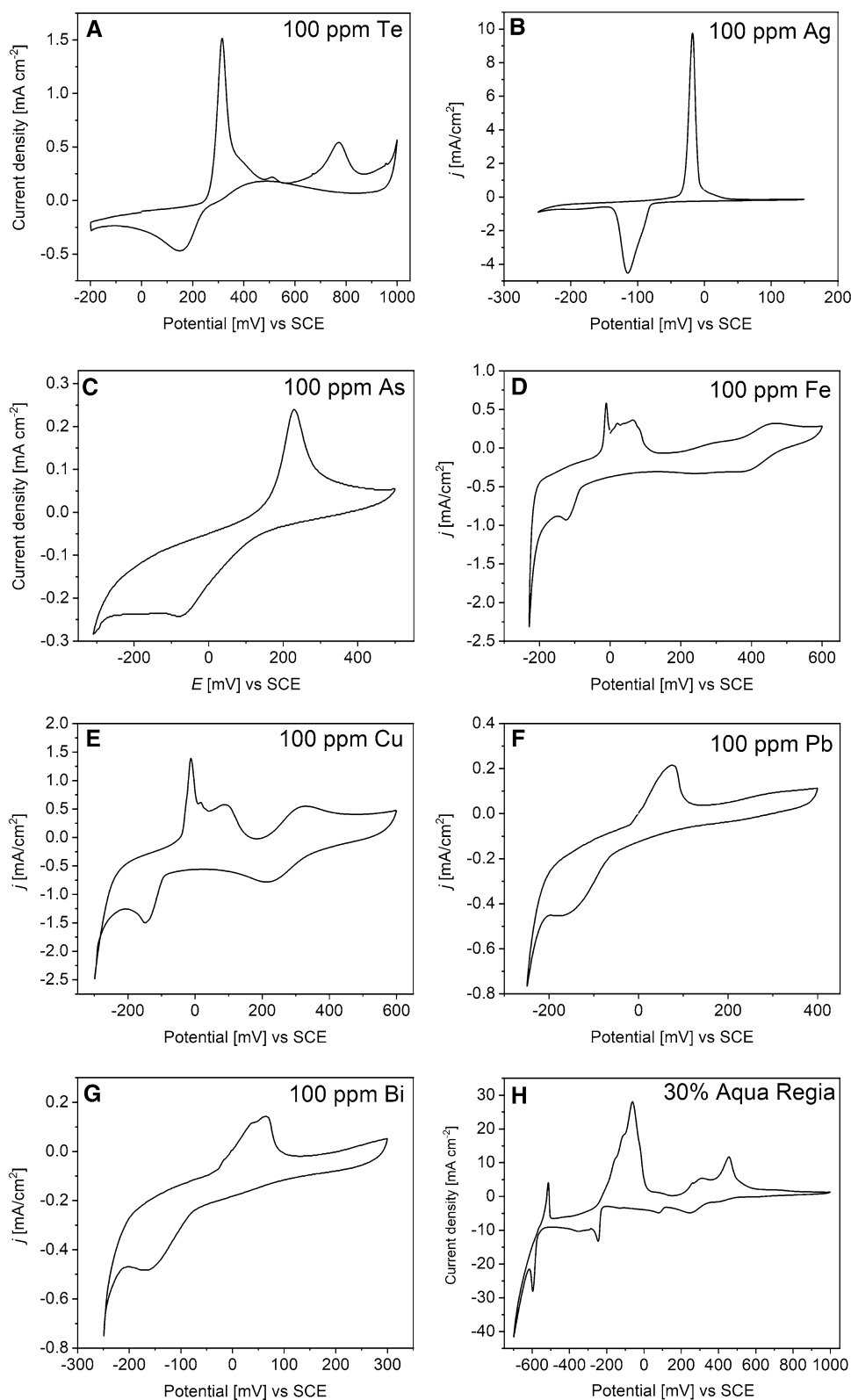
3 Results and discussion

3.1 Determination of the EDRR and EW parameters

As it can be seen in Table 1, Doré slag PLS has a complex composition due to the presence of a large number of metal species. The elements with the g dm⁻³ concentrations originate from the slag forming agents (Na, B, As) and anode slime (Ba, Bi, Cu, As, Pb, Fe), although other elements present in the anode slime are also detected at appreciable ppm or ppb levels including Mg, Al, Te and Sb. Prior to electrochemical recovery experiments being conducted, cyclic voltammetry (CV) measurements were carried out in individual 100 ppm synthetic solutions of Te, Ag, Cu, Fe, Bi, Pb and As in 30% aqua regia (Fig. 1a–i) as well as Doré slag PLS (Fig. 1h), in order to determine the Te deposition/stripping peaks and potential sacrificial elements.

As can be seen in Fig. 1a, the deposition of Te commences at approximately +250 mV versus SCE and has a peak centred at +75 mV versus SCE. These values are in

Fig. 1 Cyclic voltammetry (CV) measurements of synthetic solutions composed of 30% aqua regia and 100 ppm of **a** Te, **b** Ag, **c** As, **d** Fe, **e** Cu, **f** Pb, **g** Bi and **h** Doré slag PLS. (Scan rate = 10 mV/s and starting potential = 0 mV vs. SCE)



good correlation with the literature [44, 45]. The reduction and oxidation peaks of Ag (Fig. 1b) in 30% aqua regia are around -110 and -25 mV versus SCE, respectively. For As,

the reduction showed a peak around -50 mV, Fig. 1c. Iron showed a reduction peak around -100 mV, whereas another reduction peak was found approximately at $+400$ mV, which

relate to $\text{Fe}^0/\text{Fe}^{2+}$ and $\text{Fe}^{2+}/\text{Fe}^{3+}$, respectively (Fig. 1d). For Cu, two reduction peaks around -150 mV and $+200$ mV (Fig. 1e) correspond to Cu^0/Cu^+ and $\text{Cu}^+/\text{Cu}^{2+}$. However, as the aqua regia media includes also chlorides, the dissolved copper is most likely complexed with chlorides, e.g. as CuCl^+ and CuCl_2^- , rather than ions [46]. The reduction peak for Pb was determined to be around -150 mV (Fig. 1f), whereas the CV of Bi—shown in Fig. 1g—highlights that although the Bi reduction potential is similar to that of Pb, the oxidation is at around $+75$ mV. In addition, a CV was measured using the Doré slag PLS as the electrolyte (Fig. 1h) and this shows a wide number of peaks as a result of the complex combination of elements within the solution. For example, depending on pH, Te has a number of oxidation stages [47, 48] and can form complexes with other metals like bismuth, silver and/or copper [7, 8, 49–54]. Based on the results from the CV investigations, the E_1 (deposition) potentials and E_2 (cut-off) potentials—outlined in Table 2—were selected as the ED RR parameters in the multimetal PLS electrolyte.

As tellurium electrowinning has been previously investigated under different pH conditions [55–59], this information, along with the findings from the PLS CV measurements (Fig. 1h), was used to select the EW experimental potentials shown in Table 3. Previous research [55–59] has demonstrated that along with pH, the choice of electrolyte and presence of other elements all affect the deposition potentials of tellurium.

Cyclic voltammograms (Fig. 1a–h) together with existing literature [41–48] highlight that copper would be the most beneficial candidate to act as a sacrificial element in ED RR, especially as chloride-based solutions decrease Cu reduction potential (-150 mV vs. SCE, Fig. 1e) due to the formation of monovalent (Cu^+) copper chloride complexes. This provides a unique advantage in selective Te recovery; for example, the reduction potential in the current study is ca. 243 mV lower compared to non-chloride solution ($+93$ mV vs. SCE, standard electrode potential). Such values are of a similar magnitude to the calculations previously outlined by Lundström et al. [46] (220 mV decrease with $[\text{Cl}^-] \sim 2.9 \text{ mol dm}^{-3}$). This theoretical background highly supports the development of electrochemical Te recovery in chloride media, as the reduction potentials of Te and Cu are not overlapping, but the nobility difference supports both direct recovery (EW) as well as the recovery through electrodeposition followed by spontaneous redox replacement (ED RR).

3.2 Tellurium recovery by ED RR from PLS

Investigation of the ED RR method to recover Te from Doré PLS initially involved the optimisation of the ED RR parameters, i.e. deposition potential (E_1), cut-off potential (E_2),

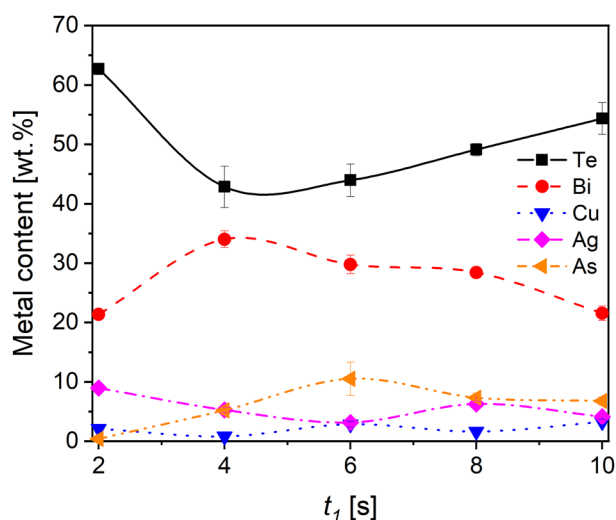


Fig. 2 Quantitative SEM-EDS results of the electrode surface metal deposits after ED RR experiments at $E_1 = -500$ mV and $E_2 = +150$ mV versus SCE, $t_1 = 2$ –10 s and $n = 100$. N.B. Pt electrode background signal is excluded from the results

deposition time (t_1), cut-off time (t_2) and number of cycles (n). More information about the definition of these parameters has been published earlier [37–41]. Five deposition times, t_1 , were studied in the range of 2–10 s, along with the four deposition potentials, E_1 and three cut-off potentials, E_2 , presented in Table 2. Cut-off time, t_2 , and the number of cycles, n , were kept constant at 1000 s and 100, respectively.

The effect of deposition time, t_1 , is presented in Fig. 2. As can be observed, the content of Te is found to be highest when the deposition time is shortest, although after the minimum level at $t_1 = 4$ s, the level of Te steadily increases up to $t_1 = 10$ s. In terms of energy consumption, shorter deposition times are preferable, particularly as the effect of hydrogen evolution can be minimised. Additionally, with the shortest t_1 the amount of other elements deposited was reduced and Te was more evenly distributed across the electrode surface. During the RR (redox replacement) stage, on the other hand, smaller particles may spontaneously re-dissolve into the electrolyte before being redeposited on larger particles via Ostwald ripening [60–62], and actually, this re-nucleation process enhances Te electrodeposition due to uniform and larger Te particle size. Based on these findings, a deposition time (t_1) of 2 s was selected for further investigation into the effect of deposition and cut-off potentials (E_1 and E_2). The results of these parameters are shown in Fig. 3.

With a more anodic deposition potential ($E_1 = -100$ mV, Fig. 3a), the amount of Te detected is relatively modest ($< 40\%$) when compared with experiments conducted at more cathodic potentials (Fig. 3b, c). This observation is primarily as a result of the increased deposition levels of the sacrificial metals that occur as the deposition potential

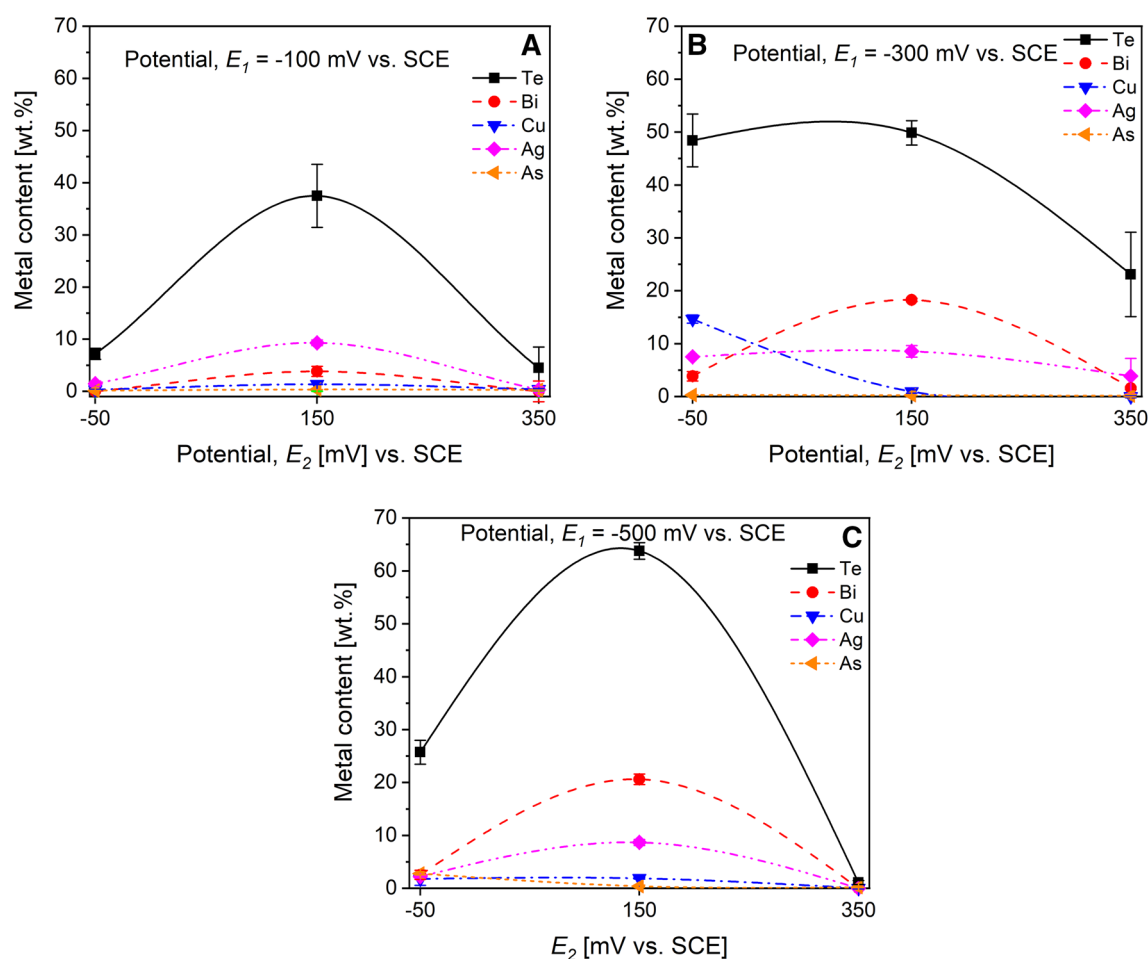


Fig. 3 Metal recoveries obtained after EDRR experiments at different ED potentials (E_1) as a function of cut-off potential (E_2): **a** $E_1 = -100$ mV, **b** $E_1 = -300$ mV and **c** $E_1 = -500$ mV. $t_1 = 2$ s and $n = 100$. All potentials are versus SCE

(E_1) is shifted more cathodically from -100 to -500 mV. Consequently, the levels of Te enrichment measured are highest when cut-off potential $E_2 = +150$ mV, as this potential appears to provide a more optimum cut-off time for the redox replacement. At $E_2 > +200$ mV, i.e. higher than the Te stripping potential, any redox-replaced Te present on the surface re-dissolves (Fig. 1a), whilst at the lower cut-off potential (-50 mV) there is insufficient time for Te to fully replace the sacrificial metal deposited. In addition, as smaller particles tend to dissolve back into solution due to Ostwald ripening, a too low cut-off potential prevents re-nucleation on the electrode surface prior to the next EDRR cycle. Results in Fig. 3 demonstrate that the highest level of Te enrichment (approx. 64 wt%) is achieved when $E_1 = -500$ mV and $E_2 = +150$ mV. Additional measurements that used an E_2 value $= +75$ mV versus SCE—the value of Te reduction peak in Fig. 1a—were performed (Table 4). However, this cut-off potential only gave rise to 42 wt% Te, most likely due to an incomplete redox replacement process. In order to maximise the Te recovery both in EW

Table 4 Quantitative SEM-EDS results of the electrode surface metal deposits after EDRR experiments at $E_1 = -500$ mV and $E_2 = +75$ mV or $+150$ mV, $t_1 = 2$ s and $n = 100$

E_2 [mV vs. SCE]	Te (wt %)	Bi (wt %)	Cu (wt %)	Ag (wt %)	As (wt %)
+75	41.95	29.19	0.99	4.52	5.92
+150	63.77	20.62	1.89	8.67	0.40

Pt electrode background signal is excluded from the results

and EDRR, $E = +75$ mV was selected to be used only in the EW experiments and a higher potential of $E_2 = +150$ mV was employed in the EDRR experiments.

Figure 3 also highlights that both Ag and Bi behave in a similar way to Te, although Ag and Bi are detected in lower amounts at the electrode surface. The ratio between Ag and Te found on the electrode is similar to that found in the original solution, where the Te concentration is ca. 8 times higher, which suggests comparable electrochemical behaviour. The presence of Ag, As, Bi and Cu on the surface

Table 5 Quantitative SEM–EDS results of the metals deposits on the surface of the employed electrode after EW experiments at different potentials and duration = 1200 s

Potential (mV vs. SCE)	Te (wt %)	Bi (wt %)	Cu (wt %)	Ag (wt %)	As (wt %)
–600	3.5	44.0	34.3	0.5	1.2
–500	3.3	35.8	39.1	0.6	0.5
–360	2.6	32.8	48.7	0.3	0.7
–245	12.8	59.3	14.5	1.9	0.5
+75	55.1	17.4	1.6	1.9	2.9
+150	4.3	18.1	0.0	32.2	0.5
+250	0.4	42.2	0.0	10.4	3.7

Pt electrode background signal is excluded from the results

is probably due to tellurium's ability to form several different alloys with other elements [7, 8, 49–54]. If tellurium is deposited as an alloy, the alloying element can be replaced with another tellurium ion which promotes tellurium recovery as Te is the most noble element in the solution (with the exception of silver) [63]. Consequently, there exist two pathways for Te deposition, which occur simultaneously, leading to increased levels of Te at the surface: the redox replacement reaction of alloying elements resulting in Te alloys and redox replacement of metallic sacrificial element, resulting in metallic Te recovery. Therefore, the content of tellurium detected on the surface is the combination of a pure tellurium and telluride alloying, and the possible tellurides could include for example, Ag_2Te [64] and Bi_2Te_3 [65].

In the case of Bi, on the other hand, a different behaviour is observed: even though Bi concentration in the PLS solution is significantly higher (4.6 g dm^{-3}), the level detected after EDRR is considerably lower relative to Te. During the RR phase, one limiting factor is mass-transport of electrolyte to the surface of the electrode, whereas at the electrode surface, the reaction rate is dictated by the metal reduction potential differences—the higher the reduction potential difference, the more likely the redox replacement. Consequently as both Te and Ag have similar reduction potentials, it is possible that during the RR step, both these elements replace the sacrificial Cu and to a lesser extent Bi (see Fig. 3 and Table 4).

3.3 Tellurium recovery by EW from PLS

The differences in recovery efficiency between EW and EDRR were investigated by performing EW over a potential range between –600 to +250 mV. It can be seen that in EW operation (Table 5), Te content remains almost constant at ca. 3–3.5%, when the deposition potentials are $\leq -360 \text{ mV}$, as the solution is rich in Cu/Bi and the deposition of these elements predominates at these more cathodic potentials,

(Fig. 1e, g). At potentials $> -245 \text{ mV}$, the level of Te detected begins to increase significantly—to a maximum of 55 wt % at—as the deposition of Bi and Cu reduces and Te reduction starts to dominate, reduction peak of Te being at +75 mV (Fig. 1a). At higher potentials, Te reduction is less likely, and therefore +75 mV was selected as the optimal potential for EW recovery. Nevertheless, even at the optimal deposition potential for Te, the co-deposition of other metallic impurities—in this case Bi—was also observed and this is similar to previous findings for other EW processes [66–69].

The results in Table 5 demonstrate that although notable Te enrichment is achievable by optimised EW operation with 1200 s duration, the comparative active deposition time for EDRR is only 200 s ($n = 100$, $t_1 = 2 \text{ s}$) and provides a higher level of Te enrichment (Fig. 2). Overall, these findings clearly indicate that relatively selective Te recovery from Doré slag PLS can be achieved with both optimised EDRR and EW methodologies.

3.4 Morphology of tellurium deposits achieved by EDRR and EW

During both EDRR and EW, the metals deposited on the electrode surface were found to be porous in nature and scattered around the area exposed to the electrolyte. Moreover, different metals displayed diverse behaviours, for example, Ag and Cu were found to be enriched in separate areas away from Te, whereas Bi and As were spread across the whole reaction area. This was confirmed by quantitative SEM–EDS analysis. Figure 4a shows a SE (secondary electron) micrograph after an optimised Te deposition EDRR experiment. The bright, elevated areas are mostly comprised of Te (~64 wt%) and Bi (~21 wt%)—with some Ag (see Fig. 2)—whilst the darker, flat surface is composed of the Pt electrode material. As can be seen at higher magnification (Fig. 4b), the Te and Bi deposits are porous in nature and tend to form dendritic-type structures, as previously is observed for both elements in electrodeposition studies [70, 71]. Moreover, it is known that the application of an overpotential can lead to dendrite growth [72] and in this case, the dendritic growth is most likely due to the overpotential applied during the electrodeposition of the sacrificial elements (mostly Cu) as has been shown previously for copper [72–76]. After the deposition of the sacrificial elements, the redox replacement process is followed and the dendritic structure remains as tellurium replaces the sacrificial elements on the electrode surface wherever they have been deposited, i.e. on the inhomogeneous surface areas [37, 41, 77]. Nonetheless in this case, Te is recovered via redox replacement and therefore, it is possible that tellurium can spontaneously forms dendrites. Such a phenomenon is fairly unlikely however, as no external energy is applied and therefore tellurium maintains the

Fig. 4 Representative SE micrographs of the Pt electrode surface after an optimised Te deposition EDRR experiment ($E_1 = -500$ mV and $E_2 = +150$ mV vs. SCE, $t_1 = 2$ s and $n = 100$) at **a** 1000 \times and **b** 7000 \times magnification

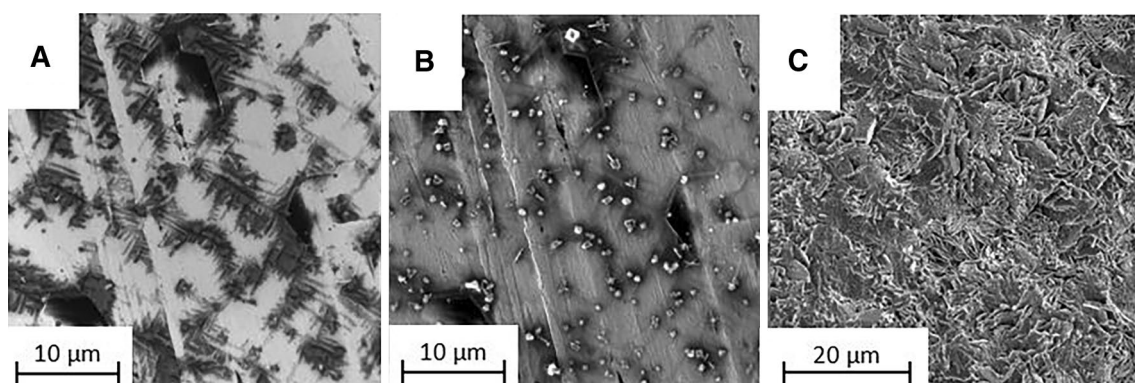
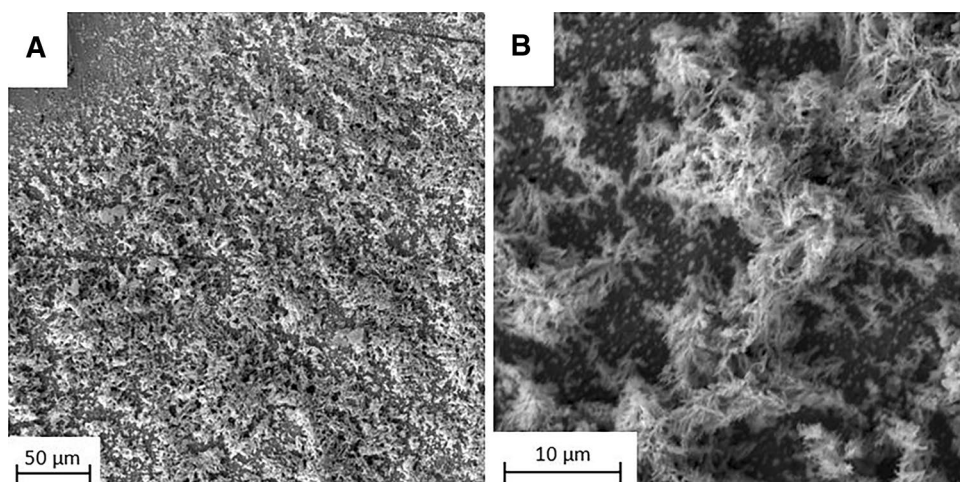


Fig. 5 SEM–BSE (**a**) and SE (**b**) micrographs (magnification 2000 \times) of the Pt electrode after 200 s and SE micrograph of the Pt electrode after 72 h (**c**) (magnification 1000 \times) of optimised EW at $E = +75$ mV

same appearance as the sacrificial elements formed during electrodeposition step.

Figure 5a, b shows the surface morphology of Te present on the Pt electrode an optimised EW experiment ($E = +75$ mV) after 200-s deposition time—the same time as used in the EDRR method. According to SEM–EDS, the Te content on the electrode surface was only approx. 8 wt% *cf.* 64 wt% achieved with EDRR, although a smaller number of similar dendritic-like structures are observed as with EDRR (Fig. 4b). Nonetheless, as the magnitude of these Te deposits was almost at the limit of visual detection, their appearance could only be observed clearly with the BSE detector (Fig. 5a). In contrast, the SE micrograph shown in Fig. 5b shows the presence of associated Ag/AgCl crystals on the surface, which appear to act as surface initiation points for the Te deposition. Furthermore, the dendritic-like structure formed during tellurium EW is once again observed with longer experimental durations due to overpotential applied—as has been observed also previously [78–80]. This also indicates that the dendritic structure found after EDRR is originally formed by the sacrificial elements during the

electrodeposition step. Moreover, as 200 s was relatively short time for EW, a longer experiment was also carried out in similar conditions at the same deposition potential. Figure 5c shows the surface morphology after this longer (72 h) EW experiment conducted at optimised potential. As it can be seen, the surface is rather thick and the deposited material has grown over the whole area immersed. With a longer EW experimental time of 72 h (Fig. 5c), a thick metal layer is deposited on the surface that comprises of a majority of Te (57 wt%), although relatively high amounts of Ag (29 wt%) and Cu (6 wt%) were also detected. However, the content of bismuth was rather low, 1.3 wt%.

3.5 Combining EW and EDRR for tellurium recovery from Doré slag

Detailed investigations of the EW process for tellurium were carried out with synthetic solutions that contained 30% aqua regia and Te concentrations between 400 and 1 ppm (Fig. 6). It is noteworthy that, in conventional tellurium EW, tellurium solution concentrations are clearly higher and typically

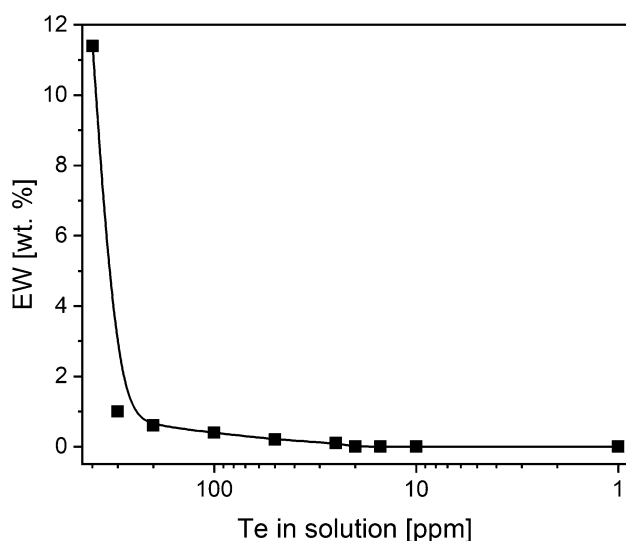


Fig. 6 Quantitative SEM–EDS of the metal deposits on a Pt electrode surface after EW experiments in a 30% aqua regia/Te only electrolyte solution ($E = +75$ mV vs. SCE and $t = 200$ s)

vary between a few tens of g dm^{-3} to several hundreds of g dm^{-3} , with impurities like Cu, Bi and Sb that create challenging process conditions due to their co-deposition with tellurium [57, 81, 82] and Table 5.

Results in Fig. 6 show that when the synthetic solution has approximately the same Te content as the original PLS (400 ppm *cf.* 421 ppm) the level of Te deposition on the Pt electrode surface is relatively high after only 200 s. However, as concentration is reduced to ≤ 300 ppm Te, the amount recovered drops dramatically. As a result, the energy efficiency of EW becomes critical when compared to the level of tellurium recovered, due to the mass-transport limited reactions that comprise the EW process, as with more

dilute solutions longer time is required for a critical mass of ions to reach the electrode surface.

Consequently, the EDRR methodology is more effective at lower concentrations than conventional EW as the metal redox replacement does not require any external applied energy, but occurs spontaneously due to reduction potential differences. For example, EDRR has already been proved to be capable of recovering Pt from acidic, sulfate-based industrial hydrometallurgical solutions in the ppb range [41]. On the other hand, the energy efficiency of EDRR process is reduced by the capacitive double-layer charging that occurs at the commencement of each ED cycle, i.e. hundreds or thousands of times, depending on the number of cycles applied [83, 84]. In comparison, the EW method only undergoes a short period of capacitive double-layer charging at the start of the process.

These findings indicate that it may be beneficial to combine EW and EDRR operation in series, Fig. 7. In the presented approach, the Doré slag PLS (PLS 1) is subjected first to EW (stage 1) until the Te concentration of the solution (PLS 2) is too low for EW (≤ 300 ppm) to be energy efficient; EDRR (stage 2) is then performed with PLS 2 in order to recover the remaining Te still present within the electrolyte. A number of experiments with extended durations were conducted with Doré slag PLS that included EW only (96 h, Stage 1), EDRR only (96 h, Stage 2) and a combined approach—total duration of 192 h—in which the initial 96 h was performed utilising EW and the remaining 96 h with EDRR. The duration of 96 h of EW was selected to ensure that the tellurium content in the Doré PLS was decreased to a level where the EW method was no longer suitable for recovery. Similar, long-lasting EW procedures for Te have been performed earlier [56, 85], where the total time for EW has been several hours. Nevertheless, in those studies the

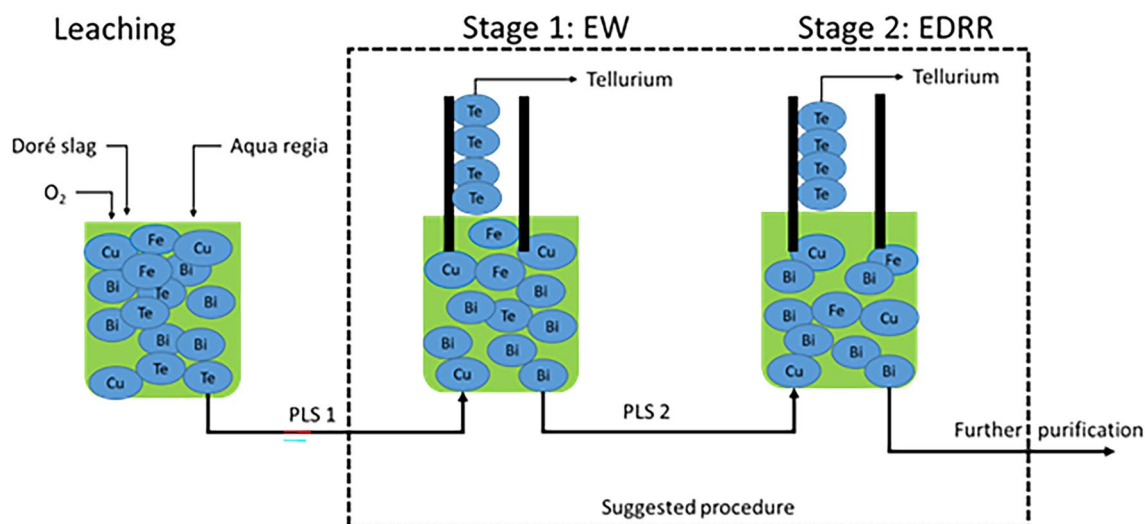


Fig. 7 Schematic of the proposed route for tellurium recovery from Doré slag

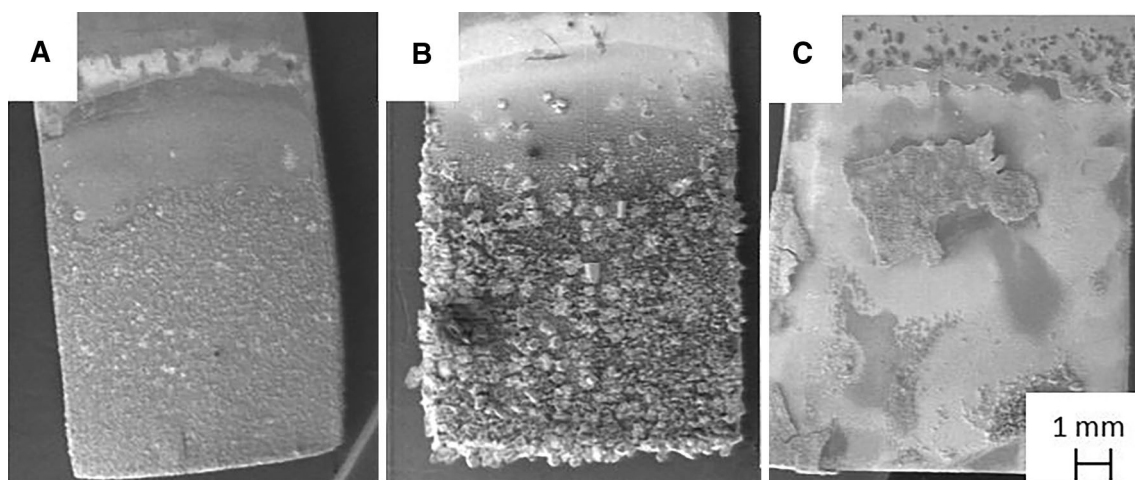


Fig. 8 SEM micrographs of Pt electrode surfaces after **a** EW, **b** EDRR and **c** combined EW-EDRR at a magnification of 8×

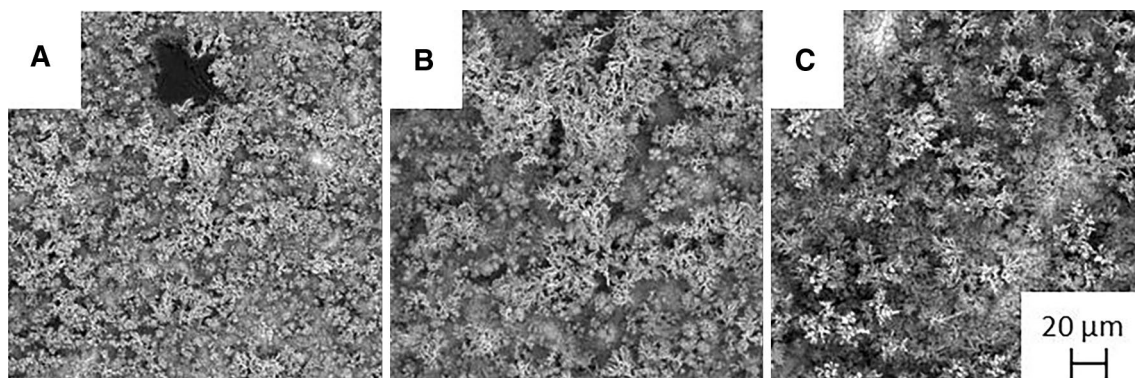


Fig. 9 SEM micrographs of Pt electrode surfaces after **a** EW, **b** EDRR and **c** combined EW-EDRR (c) at a magnification of 2000×

content of Te in the solution was several g dm^{-3} and EW was stopped when the Te content was below g dm^{-3} .

SEM micrographs obtained of the electrode surfaces after the three different methodologies used are displayed in Figs. 8 and 9. As it can be seen in Fig. 8a (=96 h EW deposition only), on the macroscale, the surface of the electrode is rather smooth compared to the other two (Fig. 8b—96 h EDRR only, and c—96 h EW + 96 h EDRR). The difference between the two electrodes used in the EW only (Fig. 8a) and EDRR only (Fig. 8b) experiments clearly highlights how the two electrochemical methods differ from each other and Fig. 8b, in particular, demonstrates Ostwald ripening. On the other hand, the morphology shown after the combined EW-EDRR process in Fig. 8c clearly has aspects of both electrochemical methods.

A more detailed morphology of the different electrode surfaces is shown in Fig. 9. As can be seen, all show similar types of dendritic-like growth, although when EW only is employed (Fig. 9a, Stage 1) the tellurium deposits are spread across the whole active electrode area, whilst in contrast,

EDRR from depleted Te solution (Fig. 9b, Stage 2) shows more compact areas of deposition. Moreover, when compared to the combined method, Fig. 9c, it is evident that tellurium can re-dissolve back to the electrolyte, most likely during the RR (redox replacement) step and such dissolution can be a limiting factor in an EDRR-based process. As seen previously, dendritic-like structures were again observed with these long-term EW, EDRR and EW-EDRR measurements and as stated earlier, they are most likely a direct result of the applied overpotential where either sacrificial elements are deposited on the electrode or, during EW, tellurium is deposited.

Table 6 presents data obtained by SEM-EDS after the EW, EDRR and combined EW-EDRR experiments performed with Doré slag PLS. After the 96-h EW experiment, the content of Te on the electrode surface is > 60%, whereas the levels of Bi and As are below 1 wt%. Furthermore, when comparing to EW performed for only 1200 s (Table 5), the content of tellurium only increased by approx. 6 wt%. In comparison, the EDRR performed for an equivalent duration

Table 6 Quantitative SEM–EDS results of the metal deposits on the Pt electrode surfaces after the EW only (Stage 1, 96 h), EDRR only (Stage 2, 96 h) and combined EW-EDRR (Stage 1 + 2, 192 h) experiments performed under optimum conditions

Sample	Te (wt %)	Bi (wt %)	Cu (wt %)	Ag (wt %)	As (wt %)
Stage 1: EW	61.51	0.79	10.37	26.98	0.34
Stage 2: EDRR	17.23	2.58	7.33	24.42	48.43
Combined: EW + EDRR	37.60	3.77	15.96	20.06	22.61

(96 h) in the Te-depleted electrolyte under optimal conditions, resulted in a significantly lower tellurium content than that achieved by EW. Nevertheless, when keeping in mind that a majority of the tellurium is already recovered during the stage 1 (EW), the results clearly demonstrate the EDRR (stage 2) technique's ability to recover Te from solutions where only very low levels of tellurium remain.

There are currently only a few studies where tellurium recovery has been performed at similar concentrations to the one utilised here—e.g. recovery from a solution containing < 100 ppm Te by bacterial leaching [86] or 500 ppm by electrochemical methods [71]. Instead, in most cases clearly higher initial Te concentrations are utilised, e.g. 1.9–3.5 g dm⁻³ industrial solutions [87] or anode slimes with ~ 34 wt% Te [88]. Therefore, the combined EW-EDRR route outlined here offers an unparalleled method for the maximisation of Te recovery from the Doré process that enhances the drive towards a more sustainable metal circular economy.

4 Conclusions

Tellurium recovery from Doré slag PLS via combined EW-EDRR has been demonstrated to be feasible and relatively selective, even though Doré slag PLS contains notable amounts of other elements at high (g dm⁻³) concentrations. Under the optimised conditions, the recovered metal deposits on the surface contained more tellurium than any other elements combined. The highest tellurium recovery from Doré slag PLS via EW resulted in ~ 55 wt% purity in the deposits, whereas EDRR resulted in ~ 64 wt%. Based on these findings, a new Doré slag treatment circuit for tellurium recovery is proposed.

The working principles and limiting tellurium concentrations were demonstrated with synthetic solutions and the results show that above 300 ppm EW is preferred, whilst below this threshold value, EDRR should be employed. By a combination of EW and EDRR processes, the recovery of pure tellurium from Doré slag can be achieved even from ppm-level solutions.

Since tellurium is still mainly produced as a side product of a copper anode slime treatment, the processing the Doré slag with the proposed combined EW-EDRR could increase

the overall profitability of a copper factory. Moreover, in terms of circular economy and sustainable development, the recovery of even a small amount (< 300 ppm) of tellurium metal circulation for use is crucial with the ever-growing demand for metals. Furthermore, the proposed new approach can offer potential for selective tailored recovery of strategically important elements in metallurgical waste and side stream fractions.

Acknowledgements Open access funding provided by Aalto University. This work has been financed and supported by the Association of Finnish Steel and Metal Producers (METSEK-project, PH & TH) together with “NoWASTE” project (Grant 297962, KY) and Gold-Tail (Grant 319691, BW & ML) funded by Academy of Finland. The research also made use of the Academy of Finland funded “RawMATTERS Finland Infrastructure” (RAMI) based at Aalto University.

Open Access This article is distributed under the terms of the Creative Commons Attribution 4.0 International License (<http://creativecommons.org/licenses/by/4.0/>), which permits unrestricted use, distribution, and reproduction in any medium, provided you give appropriate credit to the original author(s) and the source, provide a link to the Creative Commons license, and indicate if changes were made.

References

- Babula P, Adam V, Opatrilova R, Zehnalek J, Havel L, Kizek R (2008) Uncommon heavy metals, metalloids and their plant toxicity: a review. *Environ Chem Lett* 6(4):189–213. <https://doi.org/10.1007/s10311-008-0159-9>
- U.S. Geological Survey (2018) Mineral commodity summaries 2018. U.S. Geological Survey, Reston, p 200. <https://doi.org/10.3133/70194932>
- Hoffmann JE (1989) Recovering selenium and tellurium from copper refinery slimes. *JOM* 41(7):33–38. <https://doi.org/10.1007/BF03220269>
- Fthenakis VM (2000) End-of-life management and recycling of PV modules. *Energy Policy* 28(14):1051–1058. [https://doi.org/10.1016/S0301-4215\(00\)00091-4](https://doi.org/10.1016/S0301-4215(00)00091-4)
- Feltrin A, Freundlich A (2008) Material considerations for terawatt level deployment of photovoltaics. *Renew Energy* 33(2):180–185. <https://doi.org/10.1016/j.renene.2007.05.024>
- Kavlat G, Graedel TE (2013) Global anthropogenic tellurium cycles for 1940–2010. *Resour Conserv Recycl* 76:21–26. <https://doi.org/10.1016/j.resconrec.2013.04.007>
- Aspiala M, Taskinen P (2016) Thermodynamic study of the Ag–Sb–Te system with an advanced EMF method. *J Chem Thermodyn* 93:261–266. <https://doi.org/10.1016/j.jct.2015.08.025>
- Amouyal Y (2013) On the role of lanthanum substitution defects in reducing lattice thermal conductivity of the AgSbTe₂ (P4/


- mmm) thermoelectric compound for energy conversion applications. *Comput Mater Sci* 78:98–103. <https://doi.org/10.1016/j.commat.2013.05.027>
9. Murray CB, Norris DJ, Bawendi MG (1993) Synthesis and characterization of nearly monodisperse CdE (E = sulfur, selenium, tellurium) semiconductor nanocrystallites. *J Am Chem Soc* 115(19):8706–8715. <https://doi.org/10.1021/ja00072a025>
 10. Tang G, Qian Q, Wen X, Zhou G, Chen X, Sun M, Chen D, Yang Z (2015) Phosphate glass-clad tellurium semiconductor core optical fibers. *J Alloy Compd* 633:1–4. <https://doi.org/10.1016/j.jallcom.2015.02.007>
 11. Rellick JR, McMahon CJ, Marcus HL, Palmberg PW (1971) The effect of tellurium on intergranular cohesion in iron. *Metall Mater Trans B* 2(5):1492–1494. <https://doi.org/10.1007/BF02913388>
 12. Sherwani AF, Usmani JA (2010) Life cycle assessment of solar PV based electricity generation systems: a review. *Renew Sustain Energy Rev* 14(1):540–544. <https://doi.org/10.1016/j.rser.2009.08.003>
 13. SolarPower Europe (2018) Global Market Outlook for Solar Power/2018 – 2022, Belgium, Brussels, ISBN: 9789082714319. <http://www.solarpowereurope.org>. Accessed 12 Aug 2018
 14. Biswas J, Jana RK, Kumar V, Dasgupta P, Bandyopadhyay M, Anyal SK (1998) Hydrometallurgical processing of anode slime for recovery of valuable metals. In: Bandyopadhyay A, Goswami NG, Rao PR (eds) *Environmental and Waste Management*. National Metallurgical Laboratory, Jamshedpur, pp 2016–2224
 15. Wang WK, Hoh Y-C, Chuang W-S, Shaw I-S (1981) Hydrometallurgical process for recovering precious metals from anode slime, U.S. Patent, US4293332A, 7 pages
 16. Robles-Vega A, Sanchez-Corrales VM, Castillon-Barraza F (2009) An improved hydrometallurgical route for tellurium production. *Miner Metall Process* 26(3):169–173
 17. Wang S (2011) Tellurium, its resourcefulness and recovery. *JOM* 63(8):90–93. <https://doi.org/10.1007/s11837-011-0146-7>
 18. Swinbourne DR, Barbante GG, Sheeran A (1998) Tellurium distribution in copper anode slimes smelting. *Metall Mater Trans B* 29(3):555–562. <https://doi.org/10.1007/s11663-998-0089-8>
 19. Schlesinger ME, King MJ, Sole KC, Davenport WG (2011) *Extractive metallurgy of copper*, 5th edn. Elsevier, Oxford, pp 415–426
 20. Qu D, Lee C-WJ, Uosaki K (2009) Pt nano-layer formation by redox replacement of Cu adlayer on Au(111) surface. *Bull Korean Chem Soc* 30(12):2875–2876. <https://doi.org/10.5012/bkcs.2009.30.12.2875>
 21. Mkwizu TS, Mathe MK, Cukrowski I (2010) Electrodeposition of multilayered bimetallic nanoclusters of ruthenium and platinum via surface-limited redox – replacement reactions for electrocatalytic applications. *Langmuir* 26(1):570–580. <https://doi.org/10.1021/la902219t>
 22. Mrozek MF, Xie Y, Weaver MJ (2001) Surface-enhanced Raman scattering on uniform platinum-group overlayers: preparation by redox replacement of underpotential-deposited metals on gold. *Anal Chem* 73(24):5953–5960. <https://doi.org/10.1021/ac010639i>
 23. Kim Y-G, Kim JY, Vairavapandian D, Stickney JL (2006) Platinum nanofilm formation by EC-ALE via redox replacement of UPD copper: studies using in situ scanning tunneling microscopy. *J Phys Chem B* 110(36):17998–18006. <https://doi.org/10.1021/jp063766f>
 24. Sarkar A, Manthiram A (2010) Synthesis of Pt@Cu Core – shell nanoparticles by galvanic displacement of Cu by Pt⁴⁺ ions and their application as electrocatalysts for oxygen reduction reaction in fuel cells. *J Phys Chem C* 114(10):4725–4732. <https://doi.org/10.1021/jp908933r>
 25. Wragg DA, Yliniemi K, Watson TM, Worsley DA (2013) Platinized counter electrodes for dye sensitized solar cells through the redox replacement of a low power electrodeposited lead sacrificial template. *ECS Trans* 53(24):11–17. <https://doi.org/10.1149/05324.0011ecst>
 26. Yliniemi K, Wragg D, Wilson BP, McMurray HN, Worsley DA, Schmuki P, Kontturi K (2013) Formation of Pt/Pb nanoparticles by electrodeposition and redox replacement cycles on fluorine doped tin oxide glass. *Electrochim Acta* 88:278–286. <https://doi.org/10.1016/j.electacta.2012.10.089>
 27. Herrero E, Buller LJ, Abruña HD (2001) Underpotential Deposition at Single Crystal Surfaces of Au, Pt, Ag and other materials. *Chem Rev* 101(7):1897–1930. <https://doi.org/10.1021/cr9600363>
 28. Viyannalage LT, Vasilic R, Dimitrov N (2007) Epitaxial growth of Cu on Au(111) and Ag(111) by surface limited redox replacement – an electrochemical and STM study. *J Phys Chem C* 111(10):4036–4041. <https://doi.org/10.1021/jp067168c>
 29. Fayette M, Liu Y, Bertrand D, Nutariya J, Vasiljevic N, Dimitrov N (2011) From Au to Pt via surface limited redox replacement of Pb UPD in one-cell configuration. *Langmuir* 27(9):5650–5658. <https://doi.org/10.1021/la200348s>
 30. Gokcen D, Bae S-E, Brankovic SR (2010) Stoichiometry of Pt submonolayer deposition via surface-limited redox replacement reaction. *J Electrochem Soc* 157(11):D582–D587. <https://doi.org/10.1149/1.3490416>
 31. Brankovic SR, Wang JX, Adžić RR (2001) Metal monolayer deposition by replacement of metal adlayers on electrode surfaces. *Surf Sci* 474(1–3):L173–L179. [https://doi.org/10.1016/S0039-6028\(00\)01103-1](https://doi.org/10.1016/S0039-6028(00)01103-1)
 32. Ahmadi K, Wu D, Dole N, Monteiro RO, Brankovic SR (2019) Tuning surface chemoresistivity of Au ultrathin films using metal deposition via surface-limited redox replacement of the underpotentially deposited Pb monolayer. *ACS Sens.* 4(9):2442–2449. <https://doi.org/10.1021/acssensors.9b01045>
 33. Gregory BW, Stickney JL (1991) Electrochemical atomic layer epitaxy (ECALE). *J Electroanal Chem Interfacial Electrochem* 300(1–2):543–561. [https://doi.org/10.1016/0022-0728\(91\)85415-L](https://doi.org/10.1016/0022-0728(91)85415-L)
 34. Ouendi S, Arico C, Blanchard F, Cordon J-L, Wallart X, Taberna PL, Roussel P, Clavier L, Simon P, Lethien C (2019) Synthesis of T-Nb₂O₅ thin-films deposited by atomic layer deposition for miniaturized electrochemical energy storage devices. *Energy Storage Mater* 16:581–588. <https://doi.org/10.1016/j.ensm.2018.08.022>
 35. Patil B, Satilmis B, Khalily MA, Uyar T (2019) Atomic layer deposition of NiOOH/Ni(OH)₂ on PIM-1-based N-doped carbon nanofibers for electrochemical water splitting in alkaline medium. *Chem Sustain Energy Mater* 12(7):1469–1477. <https://doi.org/10.1002/cssc.201802500>
 36. Venkatraman K, Gusley R, Lesak A, Akolkar R (2019) Electrochemistry-enabled atomic layer deposition of copper: investigation of the deposit growth rate and roughness. *J Vac Sci Technol, A* 37(2):020901-1–020901-8. <https://doi.org/10.1116/1.5079560>
 37. Halli P, Elomaa H, Wilson BP, Yliniemi K, Lundström M (2017) Improved metal circular economy-selective recovery of minor Ag concentrations from Zn process solutions. *ACS Sustain Chem Eng* 5(11):10996–11004. <https://doi.org/10.1021/acssuschemeng.7b02904>
 38. Elomaa H, Halli P, Sirviö T, Yliniemi K, Lundström A (2018) future application of pulse plating – silver recovery from hydrometallurgical bottom ash leachant. *Trans IMF* 96(5):253–257. <https://doi.org/10.1080/00202967.2018.1507320>
 39. Yliniemi K, Wang Z, Korolev I, Hannula P, Halli P, Lundström M (2018) Effect of impurities in precious metal recovery by electrodeposition-redox replacement method from industrial side-streams and process streams. *ECS Trans* 85(4):59–67. <https://doi.org/10.1149/08504.0059ecst>
 40. Korolev I, Altinkaya P, Halli P, Hannula P-M, Yliniemi K, Lundström M (2018) Electrochemical recovery of minor concentrations

- of gold from cyanide-free cupric chloride leaching solutions. *J Clean Prod* 186:840–850. <https://doi.org/10.1016/j.jclepro.2018.03.177>
41. Halli P, Heikkinen JJ, Elomaa H, Wilson BP, Jokinen V, Yliniemi K, Franssila S, Lundström M (2018) Platinum recovery from industrial process solutions by electrodeposition-redox replacement. *ACS Sustain Chem Eng* 6(11):14631–14640. <https://doi.org/10.1021/acssuschemeng.8b03224>
 42. Yliniemi K, Nguyen NT, Mohajernia S, Liu N, Wilson BP, Schmuki P, Lundström M (2018) A direct synthesis of platinum/nickel co-catalysts on titanium dioxide nanotube surface from hydrometallurgical-type process streams. *J Clean Prod* 201:39–48. <https://doi.org/10.1016/j.jclepro.2018.08.022>
 43. Halli P, Hailemariam T, Latostenmaa P, Lundström M (2018) Leaching behavior of Cu, Bi and Sb from TROF furnace Doré slag during mineral acid leaching, International Mineral Processing Congress, Moscow, Hydro- and Bio-Hydrometallurgy Section, 446–454
 44. Sorenson TA, Lister TE, Huang BM, Stickney JL (1999) A comparison of atomic layers formed by electrodeposition of selenium and tellurium scanning tunneling microscopy studies on Au(100) and Au(111). *J Electrochem Soc* 146(3):1019–1027. <https://doi.org/10.1149/1.1391715>
 45. Sorenson TA, Varazo K, Suggs DW, Stickney JL (2001) Formation of and phase transitions in electrodeposited tellurium atomic layers on Au(1 1 1). *Surf Sci* 470(3):197–214. [https://doi.org/10.1016/S0039-6028\(00\)00861-X](https://doi.org/10.1016/S0039-6028(00)00861-X)
 46. Lundström M, Aroma J, Forsén O, Hyvärinen O, Barker MH (2005) Leaching of chalcopyrite in cupric chloride solution. *Hydrometallurgy* 77(1–2):89–95. <https://doi.org/10.1016/j.hydromet.2004.10.013>
 47. Haiduc I, King RB, Newton MG (1994) Stereochemical aspects of tellurium complexes with sulfur ligands: molecular compounds and supramolecular associations. *Chem Rev* 94(2):301–326. <https://doi.org/10.1021/cr00026a002>
 48. Alekperov AI (1974) Electrochemistry of selenium and tellurium. *Russ Chem Rev* 43(4):235–250. <https://doi.org/10.1070/RC1974v043n04ABEH001803>
 49. Jayasekera S, Ritchie IM, Avraamides J (1994) A cyclic voltammetric study of the dissolution of tellurium. *Aust J Chem* 47(10):1953–1965. <https://doi.org/10.1071/CH9941953>
 50. Mori E, Baker CK, Reynolds JR, Rajeshwar K (1988) Aqueous electrochemistry of tellurium at glassy carbon and gold: a combined voltammetry-oscillating quartz crystal microgravimetry study. *J Electroanal Chem Interfacial Electrochem* 252(2):441–451. [https://doi.org/10.1016/0022-0728\(88\)80228-6](https://doi.org/10.1016/0022-0728(88)80228-6)
 51. Rudnik E, Sobesto J (2011) Cyclic voltammetric studies of tellurium in diluted HNO₃ solutions. *Arch Metall Mater* 52(2):271–277. <https://doi.org/10.2478/v10172-011-0030-z>
 52. Rudnik E, Biskup P (2014) Electrochemical behavior of tellurium in acidic nitrate solutions. *Metall Foundry Eng* 40(1):15–32. <https://doi.org/10.7494/mafe.2014.40.1.15>
 53. Mokmeli M, Dreisinger D, Wassink B (2014) Thermodynamics and kinetics study of tellurium removal with cuprous ion. *Hydrometallurgy* 147–148:20–29. <https://doi.org/10.1016/j.hydromet.2014.04.012>
 54. Mokmeli M, Dreisinger D, Wassink B (2015) Modeling of selenium and tellurium removal from copper electrowinning solution. *Hydrometallurgy* 153:12–20. <https://doi.org/10.1016/j.hydromet.2015.01.007>
 55. Kowalik R, Kutyla D, Mech K, Tokarski T, Żabiński P (2015) Electrowinning of tellurium from acidic solutions. *Arch Metall Mater* 60(2A):591–596. <https://doi.org/10.1515/amm-2015-0178>
 56. Ha Y-C, Sohn H-J, Jeong G-J, Rhee K-I (2000) Electrowinning of tellurium from alkaline leach liquor of cemented Te. *J Appl Electrochem* 30(3):315–322. <https://doi.org/10.1023/A:1003867821601>
 57. Broderick G, Handle B, Paschen P (1999) Strategies for optimal operation of the tellurium electrowinning process. *Metall Mater Trans B* 30(1):5–13. <https://doi.org/10.1007/s11663-999-0001-1>
 58. Mezei A, Ashbury M, Canizares M, Molnar R, Given H (2008) Hydrometallurgical recycling of the semiconductor material from photovoltaic materials – Part two; Metal recovery, Hydrometallurgy 2008: Proceedings of the Sixth International Symposium, Phoenix, Arizona, USA, pp 224–237, ISBN: 9780873352666
 59. Sany S (2009) Optimisation of influential factors in electrowinning of tellurium by means of PLS modelling, Master's Thesis, Luleå University of Technology, p 47
 60. Voorhees PW (1985) The theory of oswald ripening. *J Stat Phys* 38(1–2):231–252. <https://doi.org/10.1007/BF01017860>
 61. Yao JH, Elder KR, Guo H, Grant M (1993) Theory and simulation of Ostwald ripening. *Phys Rev B* 47(21):14110–14125. <https://doi.org/10.1103/PhysRevB.47.14110>
 62. Kabalnov A (2001) Ostwald ripening and related phenomena. *J Dispers Sci Technol* 22(1):1–12. <https://doi.org/10.1081/DIS-100102675>
 63. Haynes WM, Lide DR, Bruno TJ (2017) CRC handbook of chemistry and physics: a ready-reference book of chemical and physical data, 97th edn. CRC Press, Boca Raton
 64. González-Ibarra AA, Nava-Alonso F, Uribe-Salas A (2019) Electrochemical study of silver telluride (Ag₂Te): anodic and cathodic potential dependent-reactions in alkaline cyanide solutions. *Hydrometallurgy* 183:230–239. <https://doi.org/10.1016/j.hydromet.2018.12.019>
 65. Zhu W, Yang JY, Gao XH, Bao SQ, Fan XA, Zhang TJ, Cui K (2005) Effect of potential on bismuth telluride thin film growth by electrochemical atomic layer epitaxy. *Electrochim Acta* 50(20):4041–4047. <https://doi.org/10.1016/j.electacta.2005.01.003>
 66. Mackinnon DJ, Brannen JM, Fenn PL (1987) Characterization of impurity effects in zinc electrowinning from industrial acid sulphate electrolyte. *J Appl Electrochem* 17(6):1129–1143. <https://doi.org/10.1007/BF01023596>
 67. Mulaudzi N, Kotze MH (2013) Direct cobalt electrowinning as an alternative to intermediate cobalt mixed hydroxide product. In: 7th Base Metals Conference of the Southern African Institute of Mining and Metallurgy, Johannesburg, South Africa, pp 209–222
 68. Lemos FA, Sobral LGS, Dutra AJB (2006) Copper electrowinning from gold plant waste streams. *Miner Eng* 19(5):388–398. <https://doi.org/10.1016/j.mineng.2005.10.019>
 69. Ettel VA, Gendron AS, Tilak BV (1975) Electrowinning copper at high current densities. *Metall Mater Trans B* 6(1):31–36. <https://doi.org/10.1007/BF02825675>
 70. Yu S, Zhang A, Wang C (2015) Preparation of dendritic Te crystals by electrodeposition: growth mechanism study. *J Electrochem Soc* 162(8):D401–D404. <https://doi.org/10.1149/2.0091509jes>
 71. Jin W, Hu M, Hu J (2018) Selective and efficient electrochemical recovery of dilute copper and tellurium from acidic chloride solutions. *ACS Sustain Chem Eng* 6(10):13378–13384. <https://doi.org/10.1021/acssuschemeng.8b03150>
 72. Popov KI, Živković PM, Nikolić N (2016) Electrochemical aspects of formation of dendrites. *Zaštita Materijala* 57(1):55–62. <https://doi.org/10.5937/ZasMat1601055P>
 73. Popov KI, Pavlović MG, Maksimović MD (1982) Comparison of the critical conditions for initiation of dendritic growth and powder formation in potentiostatic and galvanostatic copper electrodeposition. *J Appl Electrochem* 12(5):525–531. <https://doi.org/10.1007/BF00614978>
 74. Popov KI, Maksimović MD, Zečević SK, Stojić MR (1986) Surface roughening and dendritic growth in pulsating overpotential

- copper electrodeposition. *Surf Coat Technol* 27(2):117–129. [https://doi.org/10.1016/0257-8972\(86\)90122-2](https://doi.org/10.1016/0257-8972(86)90122-2)
75. Shao W, Zangari G (2009) Dendritic growth and morphology selection in copper electrodeposition from acidic sulfate solutions containing chlorides. *J Phys Chem C* 113(23):10097–10102. <https://doi.org/10.1021/jp8095456>
 76. Hoffman ZB, Gray TS, Xu Y, Lin Q, Gunnoe TB, Zangari G (2019) High selectivity towards formate production by electrochemical reduction of carbon dioxide at copper-bismuth dendrites. *Chem Sustain Energy Mater* 12(1):231–239. <https://doi.org/10.1002/cssc.201801708>
 77. Kaischew R, Mutaftschiew B (1965) Electrolytic nucleation of mercury (in German). *Electrochim Acta* 10(7):643–650. [https://doi.org/10.1016/0013-4686\(65\)87043-8](https://doi.org/10.1016/0013-4686(65)87043-8)
 78. Deslouis C, Maurin G, Pebere N, Tribollet B (1988) Investigation of tellurium electrocrystallization by EHD impedance technique. *J Appl Electrochem* 18(5):745–750. <https://doi.org/10.1007/BF01016902>
 79. Jiang Q, Liu C, Lu B, Xu J, Song H, Shi H, Mo D, Wang Z, Jiang F, Zhu Z (2015) PEDOT:PSS film: a novel flexible organic electrode for facile electrodeposition of dendritic tellurium nanostructures. *J Mater Sci* 50(14):4813–4821. <https://doi.org/10.1007/s10853-015-8818-2>
 80. Frantz C, Zhang Y, Michler J, Philippe L (2016) On the growth mechanism of electrodeposited PbTe dendrites. *CrystEngComm* 18:2319–2326. <https://doi.org/10.1039/C6CE00107F>
 81. Rhee K-I, Lee CK, Ha Y-C, Jeong G-J, Kim H-S, Sohn H-J (1999) Tellurium recovery from cemented tellurium with minimum waste disposal. *Hydrometallurgy* 53(2):189–201. [https://doi.org/10.1016/S0304-386X\(99\)00044-4](https://doi.org/10.1016/S0304-386X(99)00044-4)
 82. Handle B, Broderick G, Paschen P (1997) A statistical response surface study of the tellurium electrowinning process. *Hydrometallurgy* 46(1–2):105–120. [https://doi.org/10.1016/S0304-386X\(97\)00004-2](https://doi.org/10.1016/S0304-386X(97)00004-2)
 83. Rosen M, Flinn DR, Schuldiner S (1969) Double layer capacitance on platinum in 1 M H₂SO₄ from the reversible hydrogen potential to the oxygen formation region. *J Electrochem Soc* 116(8):1112–1116. <https://doi.org/10.1149/1.2412227>
 84. Cuartero M, Bishop J, Walker R, Acres RG, Bakker E, De Marco R, Crespo GA (2016) Evidence of double layer/capacitive charging in carbon nanomaterial-based solid contact polymeric ion-selective electrodes. *Chem Commun* 52(62):9703–9706. <https://doi.org/10.1039/C6CC04876E>
 85. Lee CK, Rhee K-I, Sohn H-J (1997) The recovery of tellurium from copper anode slimes by hydrometallurgical processes. *J Korean Inst Resour Recycl* 6(3):41–45
 86. Bonificio WD, Clarke DR (2014) Bacterial recovery and recycling of tellurium from tellurium-containing compounds by *Pseudoalteromonas* sp. EPR3. *J Appl Microbiol* 117(5):1293–1304. <https://doi.org/10.1111/jam.12629>
 87. Shibasaki T, Abe K, Takeuchi H (1992) Recovery of tellurium from decopperizing leach solution of copper refinery slimes by a fixed bed reactor. *Hydrometallurgy* 29(1–3):399–412. [https://doi.org/10.1016/0304-386X\(92\)90024-T](https://doi.org/10.1016/0304-386X(92)90024-T)
 88. Fan Y, Yang Y, Xiao Y, Zhao Z, Lei Y (2013) Recovery of tellurium from high tellurium-bearing materials by alkaline pressure leaching process: thermodynamic evaluation and experimental study. *Hydrometallurgy* 139:95–99. <https://doi.org/10.1016/j.hydromet.2013.07.005>

Publisher's Note Springer Nature remains neutral with regard to jurisdictional claims in published maps and institutional affiliations.

Affiliations

Petteri Halli¹  · Benjamin P. Wilson¹ · Taye Hailemariam¹ · Petri Latostenmaa² · Kirsi Yliniemi³ · Mari Lundström¹

¹ Department of Chemical and Metallurgical Engineering (CMET), Hydrometallurgy and Corrosion, School of Chemical Engineering, Aalto University, Otakaari 3 J, P.O. Box 12200, 00076 Aalto, Finland

² Boliden Harjavalta, Teollisuuskatu 1, 29200 Harjavalta, Finland

³ Department of Chemistry and Materials Science (CMAT), School of Chemical Engineering, Aalto University, Kemistintie 1, P.O. Box 16100, 00076 Aalto, Finland